Effects of trapped states on spectra of four-wave mixing and differential transmission

Eiichi Hanamura
Department of Applied Physics, University of Tokyo, 7-3-1 Hongo, Bunkyo-ku, Tokyo 113, Japan
(Received 25 February 1992)

Excitons are sometimes trapped at impurities in crystals and at defects on interfaces in the confined systems, such as quantum wells and microcrystallites embedded in a host matrix. We discuss these trapping effects on the third-order optical polarization under nearly resonant pumping of the exciton. First we predict an enhancement of $\chi^{(3)}(\Omega;\Omega,-\Omega,\Omega)$ by a factor $\Gamma_{n\to T}/\Gamma_{T\to g}$ multiplicatively on that enhanced by the large excitonic dipole moments. Here $\Gamma_{n\to T}$ and $\Gamma_{T\to g}$ are, respectively, the rate at which the exciton is trapped and the decay rate of the trapped electron into the ground state. In many cases, $\Gamma_{n\to T}$ is much larger than $\Gamma_{T\to g}$ so that a large enhancement of $\chi^{(3)}$ is expected. Second, the four-wave mixing spectrum $|\chi^{(3)}(2\Omega_1-\Omega_2;\Omega_1,-\Omega_2,\Omega_1)|$ under two beams Ω_1 and Ω_2 is shown to consist of three hierarchical structures as a function of $\Omega_1-\Omega_2$, i.e., the sharpest spike around $\Omega_1-\Omega_2=0$ with the linewidth $|\Omega_1-\Omega_2|=\Gamma_{T\to g}$, the steep shoulder with the center also at $\Omega_1-\Omega_2=0$ and the width Γ_n (the exciton decay rate), and the wide structure with the width Γ_{ng} around $\Omega_1=\omega_{1s}$ and $\Omega_2=\omega_{1s}$. Here Γ_{ng} is the relaxation rate of the exciton polarization and $\hbar\omega_{1s}$ the lowest exciton energy. Third, the differential transmission spectrum is found to show the strong absorption saturation peak or the sharp induced absorption dip as a function of pump-probe detuning $\Omega_2-\Omega_1$, depending upon the pump frequency Ω_1 relative to the exciton peak ω_{1s}.

I. INTRODUCTION

The third-order optical interaction of solids brings about many interesting physical phenomena. In this paper, however, we confine ourselves to the third-order processes described by the susceptibilities $\chi^{(3)}(\Omega;\Omega,-\Omega,\Omega)$, $\chi^{(3)}(2\Omega_1-\Omega_2;\Omega_1,-\Omega_2,\Omega_1)$, and $\chi^{(3)}(\Omega_2;\Omega_1,-\Omega_1,\Omega_2)$.[1] The first one includes optical Kerr effect and absorption saturation, the absolute value of the second, $|\chi^{(3)}(2\Omega_1-\Omega_2,\Omega_1,-\Omega_2,\Omega_1)|$, gives the four-wave mixing spectrum as a function of $\Omega_1-\Omega_2$, and the imaginary part of the third, $\chi^{(3)}(\Omega_2;\Omega_1,-\Omega_1,\Omega_2)$, the differential transmission spectrum. These third-order optical susceptibilities have been shown to be enhanced under nearly resonant pumping of the lowest-energy exciton.[2] This is because the exciton has mesoscopically enhanced transition dipole moment. This enhancement has been also experimentally confirmed in CuCl microcrystallites embedded in NaCl matrix[3] or glasses,[4] and in ZnSe crystal.[5]

The excitons are trapped sometimes at impurities in a crystal and at defects on the interfaces in a confined system. We will clarify in this paper how strongly the third-order optical responses are modified when the exciton is trapped at impurities and defects. Excitons in the crystal are trapped at impurities such as donors, acceptors, and isoelectronic atoms.[6] These bound excitons are observable as redshifted lines below the free exciton line in many semiconductors.[7] Several kinds of semiconductor microcrystallite show broad luminescence bands redshifted by as much as 1 eV below the exciton line.[8-10] The origins of these redshifted bands are still controversial. However, we can describe the main effects of these trapped states on the third-order nonlinear optical responses only in terms of a few relaxation constants relevant to the trapped state.

Conversely, once these relaxation constants are obtained from observation of the third-order optical responses such as four-wave mixing spectroscopy and the differential transmission spectrum, we will be able to get some information about the trapped state. In Sec. II A, we will formulate nearly degenerate four-wave mixing under also nearly resonant pumping of the lowest-energy exciton. The third-order optical polarization $\langle P^{(3)}(2\Omega_1-\Omega_2;\Omega_1,-\Omega_2,\Omega_1)\rangle$ with two incident beams with angular frequencies Ω_1 and Ω_2 is calculated in terms of the third-order density matrices of electronic system. These are obtained by the third-order perturbations in electron-radiation interactions.

The effects of the reservoirs such as the radiation vacuum and phonon fields are taken into account in terms of several longitudinal and transverse relaxation constants. In some cases, the trapped electron has a long decay time $(\Gamma_{T\to g})^{-1}$. Here $\Gamma_{T\to g}$ denotes the sum of the radiative and nonradiative decay rates of the trapped electron into the ground state. While the electron is in the trapped state, this electron is missing in the ground state and the trapped electron is inversely polarizable into the higher excited states. Both of these processes contribute to the third-order optical susceptibility and enhance it by the factor $\Gamma_{n\to T}/\Gamma_{T\to g}$. Here $\Gamma_{n\to T}$ is a trapping rate of the exciton, which is proportional to the concentration of defects and a cross section for the trapping. The decay time $(\Gamma_{T\to g})^{-1}$ of the trapped state has been observed to be on the order of microseconds in $CdS_{1-x}Se_x$ quantum wells[11] while the trapping rate of the exciton $\Gamma_{n\to T}$ may be larger than the exciton radiative decay rate $\Gamma_n\sim 10^9$ $\sec^{-1}$. This is because the emission intensity from the trapped state is much stronger than that of the free exciton.[8] As a result, we may expect the $\chi^{(3)}$ enhancement to be on the order of $\Gamma_{n\to T}/\Gamma_{T\to g}\sim 10^3$, as will be dis-

cussed in Sec. II C. Note, however, that this $\chi^{(3)}$ enhancement is possible only at the expense of a slow response time,[12] which is determined by the longest decay time $(\Gamma_{T\to g})^{-1}\sim 1$ μsec.

In Sec. II D we will discuss the four-wave mixing spectrum. First, the third-order optical polarization $\langle P^{(3)}(2\Omega_1-\Omega_2;\Omega_1,-\Omega_2,\Omega_1)\rangle$ is evaluated under nearly resonant pumping of the exciton with two beams $(\Omega_1,\mathbf{k}_1)$ and $(\Omega_2,\mathbf{k}_2)$ for the four-wave mixing at $(2\Omega_1-\Omega_2,2\mathbf{k}_1-\mathbf{k}_2)$, and with three beams $(\Omega_1,\mathbf{k}_1),(\Omega_1,-\mathbf{k}_1)$ for pump and $(\Omega_2,\mathbf{k}_2)$ for probe to generate the phase-conjugated wave at $(2\Omega_1-\Omega_2,-\mathbf{k}_2)$. Second, we insert this polarization $\langle P^{(3)}\rangle$ in the source term of the Maxwell equation. Then the signal intensity is proportional to the square of an absolute value of $\langle P^{(3)}\rangle$. We will be able to show, in Sec. II D, the spectrum $|\chi^{(3)}(2\Omega_1-\Omega_2;\Omega_1,-\Omega_2,\Omega_1)|$ as a function of $\Omega_1-\Omega_2$ to have the hierarchical structure with spectrum widths $\Gamma_{T\to g}$, Γ_n, and Γ_{ng} around $\Omega_1-\Omega_2=0$ under nearly resonant pumping of the exciton.

In Sec. III, the differential transmission spectrum is discussed also under nearly resonant pumping of the exciton. Under application of the pump beam Ω_1 and probe beam Ω_2, the differential transmission spectrum is presented by $-\mathrm{Im}\langle P^{(3)}(\Omega_2;\Omega_1,-\Omega_1,\Omega_2)\rangle$ as a function of $\Omega_1-\Omega_2$. Real and imaginary parts of the third-order optical susceptibility show complicated structures as functions of $\Omega_1-\Omega_2$ as well as of $\Omega_1-\omega_{1s}$, while the absolute value of $|\chi^{(3)}|$ has a rather simple structure. In this sense, the differential transmission spectrum has important information on the trapped state. The population grating from the trapped state $\rho_{TT}(\Omega_1-\Omega_2)$ has a strong dependence on $\Omega_1-\Omega_2$ in the same way as in the four-wave mixing. This hierarchical structure with two kinds of broadening Γ_n and $\Gamma_{T\to g}$ is also reflected on the differential transmission spectrum. Under the resonant pumping of the exciton $\Omega_1=\omega_{1s}$, the spectrum shows the positive peak, i.e., the absorption saturation peak at $\Omega_1-\Omega_2=0$ with the spectrum width Γ_n. When the pumping is sufficiently far off resonance, on the other hand, the induced absorption with the sharpest spectrum width $\Gamma_{T\to g}$ is expected with a sharp dip in the spectrum at $\Omega_1-\Omega_2=0$. In Sec. IV, we will discuss whether these features, due to the trapped state, have been observed already in the four-wave mixing spectrum and the differential transmission spectrum. The future problems relevant to these effects of the trapped state will be discussed also in this section.

II. NEARLY DEGENERATE FOUR-WAVE MIXING

In this section, first we will evaluate the spectrum of nearly degenerate four-wave mixing under nearly resonant pumping of the exciton $|n\rangle$ which possibly relaxes into a lower bound state $|T\rangle$. Under application of two beams $(\Omega_1,\mathbf{k}_1)$ and $(\Omega_2,\mathbf{k}_2)$, both of which are nearly resonant to the exciton, the signal at $(2\Omega_1-\Omega_2,2\mathbf{k}_1-\mathbf{k}_2)$ originating from the third-order polarization $\langle P^{(3)}(2\Omega_1-\Omega_2)\rangle$ is observed as shown in Fig. 1(a). On the other hand, when we use three incident beams, i.e., two colliding pump beams $(\Omega_1,\mathbf{k}_1)$ and $(\Omega_1,-\mathbf{k}_1)$ and probe beam $(\Omega_2,\mathbf{k}_2)$, one of the nearly degenerate four-wave mixing means generation of the phase-conjugated wave $(2\Omega_1-\Omega_2,-\mathbf{k}_2)$. Here two beams $(\Omega_1,\mathbf{k}_1)$ and $(\Omega_2,\mathbf{k}_2)$ make the population grating $\rho^{(2)}(\Omega_1-\Omega_2,\mathbf{k}_1-\mathbf{k}_2)$ and the third beam $(\Omega_1,-\mathbf{k}_1)$ is reflected by the population grating $\rho^{(2)}(\Omega_1-\Omega_2,\mathbf{k}_1-\mathbf{k}_2)$, resulting in generation of the phase-conjugated wave $(2\Omega_1-\Omega_2,-\mathbf{k}_2)$. The same phase conjugation is possible even when the roles of the two pump beams are exchanged. These processes are shown, respectively, in Figs. 1(b) and 1(c). We will evaluate the third-order polarization $\langle P^{(3)}(2\Omega_1-\Omega_2,2\mathbf{k}_1-\mathbf{k}_2)\rangle$ or $\langle P^{(3)}(2\Omega_1-\Omega_2,-\mathbf{k}_2)\rangle$ in Sec. II A, show the excitonic and trapped-state enhancement of $\chi^{(3)}(\Omega;\Omega,-\Omega,\Omega)$, respectively, in Secs. II B and II C, and clarify effects of the trapped states on the spectrum of the four-wave mixing as a function of $\Omega_1-\Omega_2$ in Sec. II D.

A. General expression

First we show the model of our electronic system in Fig. 2. The third-order optical polarization under nearly resonant pumping of the exciton in a pure crystal can be described in terms of a three-level model, i.e., a crystal

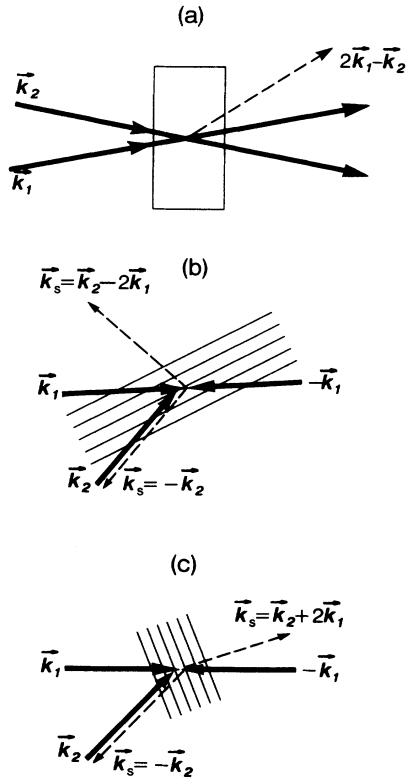

FIG. 1. (a) Nearly degenerate four-wave mixing by two incident beams $(\Omega_1,\mathbf{k}_1)$ and $(\Omega_2,\mathbf{k}_2)$ induces a signal in $(2\Omega_1-\Omega_2,2\mathbf{k}_1-\mathbf{k}_2)$. (b) and (c) Generation of phase-conjugated wave by three incident beams. (b) The third wave $(\Omega_1,-\mathbf{k}_1)$ is reflected by the population grating made by $(\Omega_1,\mathbf{k}_1)$ and $(\Omega_2,\mathbf{k}_2)$ into the phase-conjugated wave $(2\Omega_1-\Omega_2,-\mathbf{k}_2)$ and the four-wave mixing $(2\Omega_1-\Omega_2,\mathbf{k}_2-2\mathbf{k}_1)$, and (c) the third wave $(\Omega_1,\mathbf{k}_1)$ is reflected by the population grating made by $(\Omega_1,-\mathbf{k}_1)$ and $(\Omega_2,\mathbf{k}_2)$.

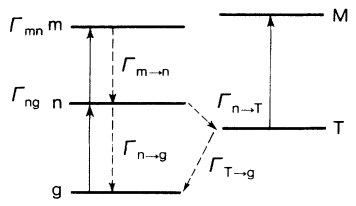

FIG. 2. Energy diagram of the electronic system in a semiconductor microcrystallite. g is the ground state, n is the one-exciton state, m is the two-exciton state, T is the one-exciton trapped state, and M is the state connected from the T state by a one-photon transition. Γ_{ng} and Γ_{mn} are transverse relaxation constants and $\Gamma_{n\to g}$, $\Gamma_{n\to T}$, and $\Gamma_{T\to g}$ are longitudinal ones.

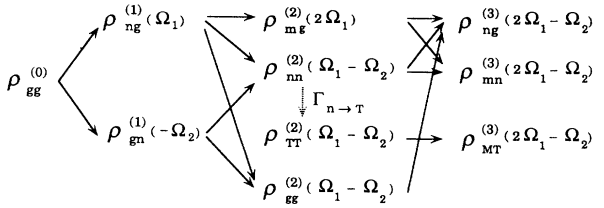

FIG. 3. The development of the density matrix of electronic system due to its perturbation of the external fields with angular frequency Ω_1 and Ω_2 for four-wave mixing and generation of phase-conjugated wave.

ground state $|g\rangle$, a single-exciton state $|n\rangle$, and a two-exciton state $|m\rangle$. This exciton in the state $|n\rangle$ possibly relaxes into the trapped state $|T\rangle$ by emitting phonons, the rate of which is described by the longitudinal decay rate $\Gamma_{n\to T}$. The exciton state $|n\rangle$ and the trapped state $|T\rangle$ decay into the ground state $|g\rangle$ radiatively or nonradiatively by emitting a photon or phonons. These rates are presented by the longitudinal decay rates $\Gamma_{n\to g}$ and $\Gamma_{T\to g}$, respectively. This trapped electron in $|T\rangle$ is connected to the higher excited states $|M\rangle$ by one-photon transition. We also introduce three transverse relaxation rates Γ_{ng}, Γ_{mn}, and Γ_{TM}, corresponding to each transition dipole moment. Effects of the reservoirs, i.e., radiation vacuum and phonon fields, are taken into account by these longitudinal and transverse relaxation constants.

The density matrix $\rho(t)$ of the electronic system obeys the following equation of motion:[13]

$$\frac{\partial\rho}{\partial t}=\frac{1}{i\hbar}[H_0+H',\rho(t)]+\left[\frac{\partial\rho}{\partial t}\right]_{\text{relax}}, \tag{2.1}$$

where H_0 denotes the Hamiltonian of the electronic system and $H'=-\mathbf{P}\cdot\mathbf{E}$ describes the interaction between the external field $\mathbf{E}=2\mathbf{E}_1\cos(\Omega_1 t-\mathbf{k}_1\cdot\mathbf{r})+2\mathbf{E}\cos(\Omega_2 t-\mathbf{k}_2\cdot\mathbf{r})$ and the electric dipole moment $\mathbf{P}=-e\sum_i\mathbf{r}_i$ of the electronic system H_0. The density matrices are obtained iteratively with respect to the interaction Hamiltonian H'. We show in Fig. 3 the progression of density matrices in each step of the perturbation to third order in H' under the rotating-wave approximation.

(1) To first order in H', only two off-diagonal components contribute:

$$\frac{\partial\rho_{ng}^{(1)}}{\partial t}=\frac{1}{i\hbar}(\hbar\omega_{ng}\rho_{ng}^{(1)}+H'_{ng}\rho_{gg}^{(0)})-\Gamma_{ng}\rho_{ng}^{(1)}. \tag{2.2}$$

When the pump field with a component $\exp(-i\Omega_1 t)$ works in H'_{ng}, the dominant term of $\rho_{ng}^{(1)}$ has the same time dependence $\exp(-i\Omega_1 t)$. Then we have for the stationary case

$$\rho_{ng}^{(1)}(\Omega_1)=\frac{H'_{ng}(\Omega_1)\rho_{gg}^{(0)}}{\hbar(\Omega_1-\omega_{ng}+i\Gamma_{ng})}. \tag{2.3}$$

The other component with time dependence $\exp(i\Omega_2 t)$ as shown in Fig. 3 is obtained by a similar method, corresponding to the propagation of the electronic state in the density matrices to the right, as follows:

$$\rho_{gn}^{(1)}(-\Omega_2)=\frac{\rho_{gg}^{(0)}H'_{gn}(-\Omega_2)}{\hbar(\Omega_2-\omega_{ng}-i\Gamma_{ng})}. \tag{2.4}$$

(2) In second order in H', we have an off-diagonal component $\rho_{mg}^{(2)}(2\Omega_1)$ and three diagonal ones $\rho_{nn}^{(2)}(\Omega_1-\Omega_2)$, $\rho_{gg}^{(2)}(\Omega_1-\Omega_2)$, and $\rho_{TT}^{(2)}(\Omega_1-\Omega_2)$, which contribute to the generation of four-wave mixing at $2\Omega_1-\Omega_2$, as shown in Fig. 3:

$$\frac{\partial\rho_{mg}^{(2)}}{\partial t}=\frac{1}{i\hbar}[\hbar\omega_{mg}\rho_{mg}^{(2)}(2\Omega_1)+H'_{mn}\rho_{ng}^{(1)}(\Omega_1)]-\Gamma_{mg}\rho_{mg}^{(2)}(2\Omega_1), \tag{2.5}$$

$$\frac{\partial\rho_{nn}^{(2)}}{\partial t}=\frac{1}{i\hbar}[H'_{ng}(\Omega_1)\rho_{gn}^{(1)}(-\Omega_2)-\rho_{ng}^{(1)}(\Omega_1)H'_{gn}(-\Omega_2)]-\Gamma_n\rho_{nn}^{(2)}, \tag{2.6}$$

$$\frac{\partial\rho_{gg}^{(2)}}{\partial t}=\frac{1}{i\hbar}[H'_{gn}(-\Omega_2)\rho_{ng}^{(1)}(\Omega_1)-\rho_{gn}^{(1)}(-\Omega_2)H'_{ng}(\Omega_1)]-\Gamma_{n\to g}\rho_{nn}^{(2)}(\Omega_1-\Omega_2)+\Gamma_{T\to g}\rho_{TT}^{(2)}(\Omega_1-\Omega_2), \tag{2.7}$$

$$\frac{\partial\rho_{TT}^{(2)}}{\partial t}=-\Gamma_{T\to g}\rho_{TT}^{(2)}(\Omega_1-\Omega_2)+\Gamma_{n\to T}\rho_{nn}^{(2)}(\Omega_1-\Omega_2). \tag{2.8}$$

Here $\Gamma_n=\Gamma_{n\to g}+\Gamma_{n\to T}$ and it is noted that the conservation of the population in the second order is confirmed, i.e.,

$$\frac{\partial}{\partial t}[\rho_{nn}^{(2)}+\rho_{TT}^{(2)}+\rho_{gg}^{(2)}]=0. \tag{2.9}$$

The stationary solutions of Eqs. (2.5)–(2.8) are obtained as follows:

$$\rho^{(2)}_{mg}(2\Omega_1)=\frac{H'_{mn}(\Omega_1)\rho^{(1)}_{ng}(\Omega_1)}{\hbar(2\Omega_1-\omega_{mg}+i\Gamma_{mg})}=\frac{H'_{mn}(\Omega_1)H'_{ng}(\Omega_1)\rho^{(0)}_{gg}}{\hbar^2(2\Omega_1-\omega_{mg}+i\Gamma_{mg})(\Omega_1-\omega_{ng}+i\Gamma_{ng})}\ , \tag{2.10}$$

$$\rho^{(2)}_{nn}(\Omega_1-\Omega_2)=\frac{H'_{ng}(\Omega_1)\rho^{(0)}_{gg}H'_{gn}(-\Omega_2)(2i\Gamma_{ng}+\Omega_1-\Omega_2)}{\hbar^2(\Omega_1-\omega_{ng}+i\Gamma_{ng})(\Omega_2-\omega_{ng}-i\Gamma_{ng})(i\Gamma_n+\Omega_1-\Omega_2)}\ , \tag{2.11}$$

$$\rho^{(2)}_{TT}(\Omega_1-\Omega_2)=\frac{\Gamma_{n\to T}}{\Gamma_{T\to g}-i(\Omega_1-\Omega_2)}\rho^{(2)}_{nn}(\Omega_1-\Omega_2)\ , \tag{2.12}$$

$$\rho^{(2)}_{gg}(\Omega_1-\Omega_2)=-\rho^{(2)}_{nn}(\Omega_1-\Omega_2)-\rho^{(2)}_{TT}(\Omega_1-\Omega_2)\ . \tag{2.13}$$

(3) To third order in H', the following three off-diagonal components are relevant to the present phenomena:

$$\frac{\partial}{\partial t}\rho^{(3)}_{ng}(2\Omega_1-\Omega_2)=-i(\omega_{ng}-i\Gamma_{ng})\rho^{(3)}_{ng}(2\Omega_1-\Omega_2)$$
$$+\frac{1}{i\hbar}[H'_{nm}(-\Omega_2)\rho^{(2)}_{mg}(2\Omega_1)+H'_{ng}(\Omega_1)\rho^{(2)}_{gg}(\Omega_1-\Omega_2)-\rho^{(2)}_{nn}(\Omega_1-\Omega_2)H'_{ng}(\Omega_1)]\ , \tag{2.14}$$

$$\frac{\partial}{\partial t}\rho^{(3)}_{mn}(2\Omega_1-\Omega_2)=-i(\omega_{mn}-i\Gamma_{mn})\rho^{(3)}_{mn}(2\Omega_1-\Omega_2)$$
$$+\frac{1}{i\hbar}[H'_{mn}(\Omega_1)\rho^{(2)}_{nn}(\Omega_1-\Omega_2)-\rho^{(2)}_{mg}(2\Omega_1)H'_{gn}(-\Omega_2)]\ , \tag{2.15}$$

$$\frac{\partial}{\partial t}\rho^{(3)}_{MT}(2\Omega_1-\Omega_2)=-i(\omega_{MT}-i\Gamma_{MT})\rho^{(3)}_{MT}(2\Omega_1-\Omega_2)$$
$$+\frac{1}{i\hbar}[H'_{MT}(\Omega_1)\rho^{(2)}_{TT}(\Omega_1-\Omega_2)-\rho^{(2)}_{Mg}(2\Omega_1)H'_{gT}(-\Omega_2)]\ . \tag{2.16}$$

The last term of Eq. (2.16) is neglected for simplicity because the transition dipole moment between the trapped state $|T\rangle$ and the ground state is negligibly small. Then the stationary-state solutions $\rho^{(3)}_{ng}(2\Omega_1-\Omega_2)$, $\rho^{(3)}_{mn}(2\Omega_1-\Omega_2)$, and $\rho^{(3)}_{MT}(2\Omega_1-\Omega_2)$ are solved from Eqs. (2.14)–(2.16):

$$\rho^{(3)}_{ng}(2\Omega_1-\Omega_2)=\frac{H'_{nm}(-\Omega_2)\rho^{(2)}_{mg}(2\Omega_1)-2\rho^{(2)}_{nn}(\Omega_1-\Omega_2)H'_{ng}(\Omega_1)}{\hbar(2\Omega_1-\Omega_2-\omega_{ng}+i\Gamma_{ng})}-\frac{H'_{ng}(\Omega_1)\rho^{(2)}_{TT}}{\hbar(2\Omega_1-\Omega_2-\omega_{ng}+i\Gamma_{ng})}\ , \tag{2.17}$$

$$\rho^{(3)}_{mn}(2\Omega_1-\Omega_2)=\frac{H'_{mn}(\Omega_1)\rho^{(2)}_{nn}(\Omega_1-\Omega_2)-\rho^{(2)}_{mg}(2\Omega_1)H'_{gn}(-\Omega_2)}{\hbar(2\Omega_1-\Omega_2-\omega_{mn}+i\Gamma_{mn})}\ , \tag{2.18}$$

$$\rho^{(3)}_{MT}(2\Omega_1-\Omega_2)=\frac{H'_{MT}(\Omega_1)\rho^{(2)}_{TT}(\Omega_1-\Omega_2)-\rho^{(2)}_{mg}(2\Omega_1)H'_{gn}(\Omega_1-\Omega_2)}{i\hbar[\Gamma_{MT}-i(2\Omega_1-\Omega_2-\omega_{MT})]}\ . \tag{2.19}$$

Here in deriving Eq. (2.17), we used the conservation relation Eq. (2.13).

(4) Finally, we have the expression of the third-order polarization with the frequency component $2\Omega_1-\Omega_2$ under nearly resonant pumping of the lowest-energy exciton $|n\rangle$ with the largest oscillator strength:

$$\langle P^{(3)}(2\Omega_1-\Omega_2)\rangle=\mathrm{Tr}\{P\rho^{(3)}(2\Omega_1-\Omega_2)\}$$
$$=P_{gn}\rho^{(3)}_{ng}(2\Omega_1-\Omega_2)+P_{mn}\rho^{(3)}_{nm}(2\Omega_1-\Omega_2)+P_{TM}\rho^{(3)}_{MT}(2\Omega_1-\Omega_2) \tag{2.20a}$$
$$=\frac{P_{gn}H'_{nm}(-\Omega_2)\rho^{(2)}_{mg}(2\Omega_1)-2P_{gn}\rho^{(2)}_{nn}H'_{ng}(\Omega_1)}{\hbar(2\Omega_1-\Omega_2-\omega_{ng}+i\Gamma_{ng})}+\frac{P_{nm}H'_{mn}(\Omega_1)\rho^{(2)}_{nn}-P_{nm}\rho^{(2)}_{mg}(2\Omega_1)H'_{gn}(-\Omega_2)}{\hbar(2\Omega_1-\Omega_2-\omega_{mn}+i\Gamma_{mn})}$$
$$-\frac{P_{gn}H'_{ng}(\Omega_1)\rho^{(2)}_{TT}(\Omega_1-\Omega_2)}{\hbar(2\Omega_1-\Omega_2-\omega_{ng}+i\Gamma_{ng})}+\sum_M\frac{P_{TM}H'_{MT}(\Omega_1)\rho^{(2)}_{TT}(\Omega_1-\Omega_2)}{\hbar(2\Omega_1-\Omega_2-\omega_{MT}+i\Gamma_{MT})}\ . \tag{2.20b}$$

B. Excitonic enhancement of $\chi^{(3)}$

In this section, we will review the excitonic enhancement[2] of the third-order optical polarization

$$\langle P^{(3)}(\Omega)\rangle=\chi^{(3)}(\Omega;\Omega,-\Omega,\Omega)|E|^2Ee^{-i\Omega t}\ . \tag{2.21}$$

Here we use a single beam with $\Omega_1=\Omega_2=\Omega$ and E means the electric field in the crystal, where we should take account of the local field effects induced by the external field. We choose, e.g., the lowest-energy exciton in CuCl microcrystallite (MC) as the elementary excitation responsible for the nonlinear optical responses. The exciton Bohr radius a_B is 6.7 Å in CuCl crystal. In the CuCl spherical MC with the radius R much larger than a_B, the

center-of-mass motion of the exciton is quantized as

$$E_n = E_g - E_{\text{exc}}^b + \frac{1}{2M}\left[\frac{\hbar\pi n}{R}\right]^2 \quad (n=1,2,\dots) . \tag{2.22}$$

Here we assumed the infinite potential barrier for an exciton in the matrix, and E_g is an energy gap between the valence and conduction bands of CuCl, E_{exc}^b the exciton binding energy in the lowest $(1s)$ electron-hole relative motion, and n the principal quantum number for the center-of-mass motion with the mass M within the MC of the radius R. The transition dipole moment to this exciton state from the crystal ground state

$$P_n = \frac{2\sqrt{2}}{\pi}\left[\frac{R}{a_B}\right]^{3/2}\frac{1}{n}\mu_{cv} \quad (n=1,2,\dots) \tag{2.23}$$

has a mesoscopic enhancement $(2\sqrt{2}/\pi)(R/a_B)^{3/2}$ in comparison to the band-to-band transition one μ_{cv}. It is noted that the oscillator strength is almost entirely concentrated on the lowest exciton state $(1s, n=1)$.[2,14]

The exciton in CuCl MC which is not strongly irradiated appears not to be accompanied by a trapped state. Therefore, we can evaluate the third-order optical susceptibility $\chi^{(3)}(\Omega;\Omega,-\Omega,\Omega)$ from Eqs. (2.20) and (2.21) by neglecting the contribution from the trapped state and putting $\mathbf{E}_1=\mathbf{E}_2=\mathbf{E}$ and $\Omega_1=\Omega_2=\Omega$. Under nearly resonant pumping of the lowest exciton $(1s, n=1)$ in the system without the trapped states such as in the fresh CuCl MC embedded in a host matrix NaCl, we have

$$\omega_{ng}=\omega_1, \quad \omega_{mg}=2(\omega_1+\omega_{\text{int}}), \quad \omega_{mn}=\omega_1+2\omega_{\text{int}} ,$$
$$P_{ng}=P_1, \quad P_{mn}=\sqrt{2}P_1 ,$$

and

$$\Gamma_n=2\gamma, \quad \Gamma_{ng}\equiv\Gamma=\gamma+\gamma', \quad \Gamma_{mg}=2(\gamma+\gamma') ,$$
$$\Gamma_{mn}=\Gamma+2\gamma=3\gamma+\gamma' . \tag{2.24}$$

Here we considered the case that the same kind of exciton, including the spin structure, is excited in a microcrystallite. When the second exciton has different spin structure from the first one, two excitons form the bound state,[15-17] i.e., the excitonic molecule so that $2\hbar\omega_{\text{int}} < -30$ meV in CuCl, and this contribution to $\chi^{(3)}$ under $\Omega\approx\omega_1$ is almost negligible in comparison to that of the same spin structure because of large detuning $|\Omega-\omega_1-2\omega_{\text{int}}|\ (\gg\omega_{\text{int}}\gg|\Omega-\omega_1|\sim\Gamma)$ in the denominators.

Inserting the expression of Eqs. (2.24) into the first two terms of Eq. (2.20b), we have the third-order optical susceptibility for the system of semiconductor MC's with a number density N_c as follows:

$$\chi^{(3)}(\Omega;\Omega,-\Omega,\Omega)=N_c|P_1|^4\left\{\frac{1}{\hbar^3(\Omega-\omega_1+i\Gamma)^2(\Omega-\omega_1-i\Gamma)}\right.$$
$$\left.-\frac{1}{\hbar^3(\Omega-\omega_1+i\Gamma)(\Omega-\omega_1-i\Gamma)[\Omega-\omega_1-2\omega_{\text{int}}+i(\Gamma+2\gamma)]}\right\}$$
$$\times\left\{\frac{2(\gamma+\gamma')}{\gamma}-\frac{\Omega-\omega_1-i\Gamma}{\Omega-\omega_1-\omega_{\text{int}}+i\Gamma}\right\} . \tag{2.25}$$

The mesoscopic dipole moment P_1 given by Eq. (2.23) is multiplied four times in the expression of the third-order optical polarization so that the mesoscopic enhancement of $\chi^{(3)}$ is expected under nearly resonant pumping of the exciton. As far as the exciton is considered as a harmonic oscillator or an ideal boson, it cannot contribute to any nonlinear optical responses. Here, however, three factors make the excitons in MC deviate from the harmonic oscillators: (1) two excitons with the same spin structure in a MC interact with each other through the repulsive interaction

$$\hbar\omega_{\text{int}}=\frac{13\pi}{3}\frac{E_{\text{exc}}^b a_B^3}{4\pi R^3/3}=\frac{13}{4}E_{\text{exc}}^b\left[\frac{a_B}{R}\right]^3 , \tag{2.26}$$

in the first Born approximation, and two excitons with different spin structures form the bound state of the excitonic molecule with the molecular binding energy $\hbar\omega_m^b\equiv-2\hbar\omega_{\text{int}}$, (2) the longitudinal decay rate of the exciton 2γ, and (3) the transverse relaxation rate $\Gamma\equiv\gamma+\gamma'$ with the pure dephasing constant γ'. As a result, under such nearly resonant pumping the lowest exciton $E_1\equiv\hbar\omega_1$ as $|\Omega-\omega_1|\ll\omega_{\text{int}}$ in the MC with a radius R such as $a_B<R<\lambda$, $\chi^{(3)}(\Omega;\Omega,-\Omega,\Omega)$ is evaluated as follows.[2]

(a) $\omega_{\text{int}}>|\Omega-\omega_1|>\Gamma$:

$$\chi^{(3)}=\frac{2N_c|P_1|^4}{\hbar^3(\Omega-\omega_1)^3}\left[1+\frac{\gamma'}{\gamma}\right]\propto\left[\frac{R}{a_B}\right]^3 , \tag{2.27}$$

where $N_c\equiv 3r/(4\pi R^3)$ is the number density of the MC's with r a constant volume fraction.

(b) $\omega_{\text{int}}>\Gamma>|\Omega-\omega_1|$:

$$\chi^{(3)}=-i\frac{2N_c|P_1|^4}{\hbar^3(\gamma+\gamma')^2\gamma} . \tag{2.28}$$

For case (a), $\chi^{(3)}$ is almost real and increases as R^3 because the fourth power of P_1 gives an R^6 dependence and overcomes the R^{-3} dependence of N_c. For case (b), $\chi^{(3)}$ becomes almost imaginary and increases as R^3 if the longitudinal decay rate 2γ is determined not by the superradiance but by size-independent processes. On the other hand, when the superradiative decay 2γ is dominant over

the pure dephasing γ', $|\chi^{(3)}|$ decreases as R^{-3} as R increases. For example, a system of CuCl MC's with $R=80$ Å and the volume ratio $r=10^{-3}$ will show $\mathrm{Im}\chi^{(3)}=-10^{-3}$ esu when we assume $\hbar\Gamma=0.1$ meV and $2\hbar\gamma=0.03$ meV.

Masumoto, Yamazaki, and Sugawara[3] observed the absorption saturation effects by the pump-probe method, which depend on the size of the CuCl MC's. They obtained $-\mathrm{Im}\chi^{(3)}\propto R^{2.6}$ and $\mathrm{Im}\chi^{(3)}=-10^{-3}$ esu for 0.12% CuCl MC's with radius 100 Å, nearly in agreement with the theory.[2,18] When the longitudinal relaxation rate 2γ is determined by the superradiative decay but the dephasing γ' is much larger than γ, $-\mathrm{Im}\chi^{(3)}\propto R^{0}$, while $-\mathrm{Im}\chi^{(3)}\propto R^{3}$ for the case in which 2γ is determined by other size-independent processes. From the exponential factor 2.6 observed by Masumoto, Yamazaki, and Sugawara,[3] the superradiative decay looks to contribute only partially to the longitudinal decay while Itoh's data[15] show the large quantum efficiency for the superradiative decay. Nakamura, Tokizaki, and Kataoka[4] also observed a large $\chi^{(3)}$ value under nearly resonant pumping of the exciton in CuCl-doped glasses, and they obtained the optimum size to get the largest $\chi^{(3)}$ value, which depends on the lattice temperature. As mentioned in Refs. 2 and 18, when the broadening Γ becomes larger than the quantization energy $\hbar(\omega_2-\omega_1)=3\hbar^2\pi^2/(2MR^2)$, the lowest exciton level is hybridized with higher levels with the smaller transition dipole moments. As the radius R of the microcrystallite increases, the quantization energy $\hbar(\omega_2-\omega_1)$ decreases while the phonon broadening $\hbar\Gamma$ increases so that the mesoscopic enhancement of $|\chi^{(3)}|$ is reduced by this hybridizing effect as the size R increases beyond the critical size. Then we can expect the optimum size for the largest $|\chi^{(3)}|$, which depends on detuning $|\omega_1-\Omega|$ and the lattice temperature. We have the expressions Eqs. (2.27) and (2.28) from Eq. (2.25) for the relevant case $\omega_{\mathrm{int}}\gg|\Omega-\omega_1|$ and Γ in which the mesoscopic enhancement of $\chi^{(3)}$ is realized as in Ref. 19, but the full expression (2.25) is a little different from those in Refs. 2 and 19. The present treatment fully takes into account (1) all possible contributions under rotating-wave and nearly resonant approximations and (2) the normalization of the density matrix in the closed system correctly.

C. Trapped-state enhancement of $\chi^{(3)}$ (Ref. 20)

Exciton emission line is observed at the same position as the absorption peak in the CuCl MC's embedded in a host NaCl matrix, while the much stronger emission lines of $CdS_{1-x}Se_x$ MC's show redshifts of an order of 1 eV below the absorption peaks than the nonshifted emission line does. These redshifted emission lines come from the trapped state of the MC's. Several microscopic models of these bound states have been proposed but these states have not been clearly identified yet. These trapped states may be localized at the MC surfaces so that these are sometimes called surface states. In this section, we evaluate contribution of those trapped states to $\chi^{(3)}(\Omega;\Omega,-\Omega,\Omega)$ in terms of characteristic constants of these states. In Sec. II D we will derive the signal spectrum of nearly degenerate four-wave mixing under nearly resonant pumping of the exciton. The spectrum of this signal intensity as a function of the difference frequency $\Omega_1-\Omega_2$ of two incident beams will give useful information of the bound states. This four-wave mixing spectrum gives not only many interesting physical phenomena, but also will be useful in clarifying the nature of the bound states. We will first discuss in this section three effects of the trapped states on $\chi^{(3)}(\Omega;\Omega,-\Omega,\Omega)$.

(1) In many cases, the trapped state has long decay time. Then the electron in the ground state cannot contribute to the polarization with frequency Ω while it is in the trapped state. This gives a contribution to $\chi^{(3)}$ and is represented by the third term of Eq. (2.20b), i.e.,

$$\Delta\chi_1^{(3)}=\frac{N_c|P_1|^4\Gamma_{n\to T}\Gamma}{\hbar^3\Gamma_{T\to g}\gamma(\Omega-\omega_1+i\Gamma)^2(\Omega-\omega_1-i\Gamma)}\ . \tag{2.29}$$

Note that this contribution is the product of the dominant term in Eq. (2.25) and a factor $\Gamma_{n\to T}/\Gamma_{T\to g}$, i.e., the factor measuring how long the excitation persists in the trapped state. The imaginary part of this term describes enhanced saturation of the absorption around $\Omega=\omega_1$. The lowest excited level in $CdS_{1-x}Se_x$ MC may be different from that of CuCl because the former is on the border between the weak and strong confinements. However, the enhancement factor $\Gamma_{n\to T}/\Gamma_{T\to g}$ works independent of the detailed electronic state. Trapping time $(\Gamma_{n\to T})^{-1}$ is considered to be on the order of nanoseconds or picoseconds, while the decay time of the luminescence from the trapped state is estimated to be on the order of microseconds. If this estimation is correct, $\chi^{(3)}(\Omega;\Omega,-\Omega,\Omega)$ is enhanced by a factor of $\Gamma_{n\to T}/\Gamma_{T\to g}\sim10^3-10^6$ in comparison to the MC's without the trapped state. However, the trapped state with the longer decay time is more easily saturated so that the higher-order optical processes become nonnegligible.

(2) The second effect of the trapped state on $\chi^{(3)}$ is presented by the last term in Eq. (2.20b). This is denoted by $\Delta\chi_2^{(3)}$. When we introduce the linear susceptibility of the trapped state $\chi_T^{(1)}(\Omega)$ and the population $n_T^{(2)}$ in the trapped state, the second contribution $\Delta\chi_2^{(3)}$ is expressed as follows:

$$\Delta\chi_2^{(3)}|E|^2Ee^{-i\Omega t}=N_c\chi_T^{(1)}(\Omega)n_T^{(2)}Ee^{-i\Omega t}\ , \tag{2.30}$$

where

$$\chi_T^{(1)}=\sum_M\frac{-|P_{TM}|^2}{\hbar(\Omega-\omega_{MT}+i\Gamma_{MT})}\ , \tag{2.31}$$

$$n_T^{(2)}=\frac{|P_1E|^2\Gamma\Gamma_{n\to T}}{\hbar^2[(\Omega-\omega_1)^2+\Gamma^2]\gamma\Gamma_{T\to g}}\ . \tag{2.32}$$

Here P_{TM} denotes the transition dipole moment between the trapped state T and the higher excited state M, and Γ_{MT} the transverse relaxation rate relevant to this transition. We do not know these values at present so that we treat $\chi_T^{(1)}$ as one parameter. This contribution of Eq. (2.30) can be considered as a polarization process once

the trapped state is populated. When the nearly resonant states $\omega_{MT} \approx \Omega$ are continuously distributed, the imaginary part of $\Delta\chi_2^{(3)}$ has the sign opposite to that of $\Delta\chi_1^{(3)}$. Therefore, this imaginary part means induced absorption. It is noted that this $\Delta\chi_2^{(3)}$ has the same enhancement factor $\Gamma_{n\to T}/\Gamma_{T\to g}$ as the first contribution $\Delta\chi_1^{(3)}$.

(3) The third effect comes from the modification of the first two terms of Eq. (2.20b) because $\Gamma_n = \Gamma_{n\to g} + \Gamma_{n\to T}$ increases by a term $\Gamma_{n\to T}$ due to the presence of the trapped state. If the decay $\Gamma_{n\to g}$ is determined by the radiative process, it is of an order of nanoseconds. When the trapping rate $\Gamma_{n\to T}$ is on the same order of magnitude or smaller than $\Gamma_{n\to g}$, this third effect is negligible. For the opposite case $\Gamma_{n\to T} \gg \Gamma_{n\to g}$, the dominant part of the nontrapped state contribution described by the first two terms of Eq. (2.20b) is reduced by the factor $\Gamma_{n\to g}/(\Gamma_{n\to T}+\Gamma_{n\to g})$ in comparison to $\chi^{(3)}$ without the trapped states.

It is noted that the excitonic enhancement of $\chi^{(3)}$ is accompanied with the fast switching due to the superradiative decay, resulting in the enhancement of the figure of merit, but that the trapped-state enhancement of $\chi^{(3)}$ is accomplished at the expense of long response time, which is determined by the longest time constant $(\Gamma_{T\to g})^{-1} \sim 10^{-6}$ sec.

D. Four-wave mixing spectroscopy

The effects of the trapped state on the third-order polarization $\langle P^{(3)}(2\Omega_1-\Omega_2)\rangle$ are discussed for two cases of two- and three-beam excitations in this section. First, under application of two beams $(\Omega_1,\mathbf{k}_1)$ and $(\Omega_2,\mathbf{k}_2)$, both of which are nearly resonant to the exciton, the signal at $(2\Omega_1-\Omega_2, 2\mathbf{k}_1-\mathbf{k}_2)$ is observed, originating from the third-order polarization $\langle P^{(3)}(2\Omega_1-\Omega_2, 2\mathbf{k}_1-\mathbf{k}_2)\rangle$. This is schematically shown in Fig. 1(a). Second, under application of two pump beams $(\Omega_1, \pm\mathbf{k}_1)$ and probe beam $(\Omega_2,\mathbf{k}_2)$, the generation of the phase-conjugated wave is observed at $(2\Omega_1-\Omega_2, -\mathbf{k}_2)$ as shown in Figs. 1(b) and 1(c). In this first case, the last two terms of Eq. (2.20b) come from reflection of the beam $(\Omega_1, -\mathbf{k}_1)$ due to the population grating $\rho_{TT}^{(2)}(\Omega_1-\Omega_2, \mathbf{k}_1-\mathbf{k}_2)$ on the trapped states created by the two incident beams $(\Omega_1,\mathbf{k}_1)$ and $(\Omega_2,\mathbf{k}_2)$. In the second case, the third wave $(\Omega_1,\mathbf{k}_1)$ is reflected by the population grating $\rho_{TT}^{(2)}(\Omega_1-\Omega_2, -\mathbf{k}_1-\mathbf{k}_2)$, both resulting in generation of the phase-conjugated wave of the probe beam $(\Omega_2,\mathbf{k}_2)$ at $(2\Omega_1-\Omega_2, -\mathbf{k}_2)$. Both cases can be discussed in the same way in terms of Eq. (2.20b). The effects of the trapped states are expressed for both the cases in the following form:

$$\Delta P^{(3)}(2\Omega_1-\Omega_2) = \rho_{TT}^{(2)}(\Omega_1-\Omega_2)[-\chi_{ng}^{(1)}(\Omega_1,\Omega_2)+\chi_T^{(1)}(\Omega_1,\Omega_2)]E_1 e^{-i\Omega_1 t}, \tag{2.33}$$

where

$$\rho_{TT}^{(2)}(\Omega_1-\Omega_2) = \frac{\Gamma_{n\to T}}{\Gamma_{T\to g}-i(\Omega_1-\Omega_2)}\rho_{nn}^{(2)}(\Omega_1-\Omega_2)$$

$$= \frac{\Gamma_{n\to T}\{2\Gamma_{ng}-i(\Omega_1-\Omega_2)\}H'_{ng}(\Omega_1)\rho_{gg}^{(0)}H'_{gn}(-\Omega_2)}{\hbar^2\{\Gamma_{T\to g}-i(\Omega_1-\Omega_2)\}\{\Gamma_n-i(\Omega_1-\Omega_2)\}(\Omega_1-\omega_{ng}+i\Gamma_{ng})(\Omega_2-\omega_{ng}-i\Gamma_{ng})}, \tag{2.34}$$

$$\chi_{ng}^{(1)}(\Omega_1,\Omega_2) = \frac{-P_{ng}P_{gn}}{\hbar(2\Omega_1-\Omega_2-\omega_{ng}+i\Gamma_{ng})}, \tag{2.35}$$

$$\chi_T^{(1)}(\Omega_1,\Omega_2) = \sum_M \frac{-P_{TM}P_{MT}}{\hbar(2\Omega_1-\Omega_2-\omega_{MT}+i\Gamma_{MT})}. \tag{2.36}$$

As Eqs. (2.33) and (2.34) show, the third-order polarization has a singular behavior as a function of $\Omega_1-\Omega_2$ around the origin $\Omega_1-\Omega_2=0$ because Γ_n and $\Gamma_{T\to g}$ in the denominator of Eq. (2.34) are very small in comparison to Γ_{ng}. Here the longitudinal decay rate $\Gamma_n = \Gamma_{n\to g}+\Gamma_{n\to T}$. The decay time of the exciton $(\Gamma_n)^{-1}$ is observed to be on the order of nanoseconds, while the decay time of the trapped excitation $(\Gamma_{T\to g})^{-1}$ to be on the order of microseconds, e.g., in the case of the exciton in GaAs quantum-well systems. On the other hand, the transverse relaxation time $(\Gamma_{ng})^{-1}$ of the exciton is on the order of picoseconds. The signal of the degenerate four-wave mixing (DFWM) is proportional to the square of the absolute value of $P^{(3)}(2\Omega_1-\Omega_2)$.

Let us consider first the exciton in GaAs quantum wells and bulk crystals. In this case, the exciton-exciton interaction is negligible, because it is inversely proportional to the crystal volume, for the excitons with the same spin structure. The molecular binding energy of two excitons with different spin structure is so small in GaAs crystal that this contribution should be taken into account under nearly resonant pumping of the lowest exciton. Then we have the following expression of the third-order optical polarization:

$$\langle P^{(3)}(2\Omega_1-\Omega_2)\rangle = 2|P_{1s}|^4 E(-\Omega_2)E(\Omega_1)^2/\hbar^3$$
$$\times\left[\frac{-2i\gamma}{(2\Omega_1-\Omega_2-\omega_{1s}+i\Gamma)\{2\Omega_1-\Omega_2-\omega_{1s}+i(\Gamma+2\gamma)\}(\Omega_1-\omega_{1s}+i\Gamma)^2}\right.$$
$$\times\left\{1-\frac{2\{2\Gamma-i(\Omega_1-\Omega_2)\}(\Omega_1-\omega_{1s}+i\Gamma)}{\{2\gamma-i(\Omega_1-\Omega_2)\}(\Omega_1-\omega_{1s}-i\Gamma)}\right\}$$
$$-\frac{(2i\gamma+\omega_m^b)|P_m/P_{1s}|^2}{(2\Omega_1-\Omega_2-\omega_{1s}+i\Gamma)\{2\Omega_1-\Omega_2-\omega_{1s}+\omega_m^b+i(\Gamma+2\gamma)\}}$$
$$\times\frac{1}{(\Omega_1-\omega_{1s}-i\Gamma)}\left\{\frac{1}{\Omega_1-\omega_{1s}+\omega_m^b/2+i\Gamma}-\frac{2(2i\Gamma+\Omega_1-\Omega_2)}{(\Omega_1-\omega_{1s}-i\Gamma)(\Omega_1-\Omega_2+2i\gamma)}\right\}$$
$$+\frac{\Gamma_{n\to T}[2\Gamma-i(\Omega_1-\Omega_2)]}{[\Gamma_{T\to g}-i(\Omega_1-\Omega_2)][2\gamma-(\Omega_1-\Omega_2)](\Omega_1-\omega_{1s}+i\Gamma)(\Omega_2-\omega_{1s}-i\Gamma)}$$
$$\left.\times\left\{\frac{1}{2\Omega_1-\Omega_2-\omega_{1s}+i\Gamma}-\sum_M\frac{|P_{MT}|^2/|P_{1s}|^2}{2\Omega_1-\Omega_2-\omega_{MT}+i\Gamma_{MT}}\right\}\right], \tag{2.37}$$

where P_m is the transition dipole moment between $1s$ exciton state and the excitonic molecule (EM) state, and we use the same notations of Γ and 2γ as in Eq. (2.24). When we denote by l and a_m, respectively, the coherence length of the exciton and an average separation of two excitons in the EM, the excitonic transition dipole moment P_{1s} is on the order of $(l/a_B)^{3/2}\mu_{cv}$ in the bulk crystal, while the transition dipole moment P_m to the EM from a single $1s$ exciton is $\sim(a_m/a_B)^{3/2}\mu_{cv}$.[18,21–23] As a result, the relative magnitude of the second to the first term in the square brackets of Eq. (2.37) is estimated to be on the order of magnitude $|P_m/P_{1s}|^2(\Gamma/\omega_m^b)\sim(a_m/l)^3(\Gamma/\omega_m^b)$ under nearly resonant pumping of the $1s$ exciton $\Omega_1\sim\Omega_2\sim\omega_{1s}$. In the case of the exciton in GaAs quantum well, it is $\sim(a_m^3/l^2a_B)^{1/2}(\Gamma/\omega_m^b)$,[18,23] and $\hbar\Gamma\sim\hbar\omega_m^b\approx 1$ meV. As a result, the first term overcomes the second at such a low temperature as the exciton coherent length l is larger than the molecular extent $a_m\sim a_B$. On the other hand, the exciton in bulk CuCl crystal has large molecular binding energy $\hbar\omega_m^b\sim 30$ meV $\gg\hbar\Gamma\sim 0.02$ meV at low temperature $T\sim 4$ K. Therefore, the molecular level is so greatly detuned under nearly resonant pumping of the lowest exciton that the contribution from the EM to $\chi^{(3)}$ is almost negligible. Furthermore, the coherent length l of the exciton is much larger than the molecular extent a_m in the good crystals at low temperature. As a result, the second term in the square brackets of Eq. (2.37) is negligible in comparison to the first also under nearly resonant pumping of the lowest exciton at low temperature in the good CuCl crystals.

The signal of DFWM is proportional to the square of the absolute value of $\langle P^{(3)}(2\Omega_1-\Omega_2)\rangle$. The absolute magnitude of the third-order polarization $|\langle P^{(3)}(2\Omega_1-\Omega_2)\rangle|$ is plotted as a function of detuning $\Omega_1-\Omega_2$ in Fig. 4. As a result, the spectrum of the DFWM shows the following hierarchical structure: (1) the very sharp Lorentzian structure (like a spike) with the half-width $\Gamma_{T\to g}\sim 10^6$ sec^{-1} around $\Omega_1-\Omega_2=0$, (2) the rather sharp Lorentzian with the half-width $\Gamma_n\sim 10^9$ sec^{-1} around $\Omega_1-\Omega_2=0$, and (3) the broad structure with the width $\Gamma_{ng}\sim 10^{12}$ sec^{-1} around $\Omega_1\sim\omega_{ng}$ and $\Omega_2\sim\omega_{ng}$. These DFWM spectra have been observed by Remillard and his co-workers for the exciton in GaAs quantum-well systems.[24]

The third-order optical susceptibility $\chi^{(3)}(2\Omega_1-\Omega_2;\Omega_1,-\Omega_2,\Omega_1)$ is defined by

$$\langle P^{(3)}(2\Omega_1-\Omega_2)\rangle=\chi^{(3)}(2\Omega_1-\Omega_2;\Omega_1,-\Omega_2,\Omega_1)\times|E(\Omega_1)|^2E(-\Omega_2)\,. \tag{2.38}$$

Figure 4 describes the absolute value, the real, and the imaginary parts of the normalized third-order susceptibility $\chi^{(3)}/[|P_{1s}|^4/(\hbar\Gamma)^3]$ as a function of normalized detuning $(\Omega_1-\Omega_2)/\Gamma$. Here the linear polarizability $\chi_T^{(1)}$ of the trapped state was neglected because this does not give any qualitative changes of the four-wave mixing spectrum which is presented by $|\chi^{(3)}|$. This is mainly because the transition dipole moment P_{MT} of the trapped state has no excitonic enhancement, so that $|P_{MT}|^2/|P_{1s}|^2$ is negligibly small in the last term of Eq. (2.37). Both spectra of Figs. 4(a) and 4(b) are characterized by two hierarchical structures, i.e., the sharpest spike with the spectrum width $\Gamma_{T\to g}/\Gamma=0.001$ and the second sharpest peak with the width $\Gamma_n/\Gamma=2\gamma/\Gamma=0.2$ both at $\Omega_1-\Omega_2=0$. The third structure has the peak at $\Omega_1=\omega_{1s}$ and the width Γ. As Fig. 4(b) shows, the four-wave mixing spectrum has asymmetry and dip under off-resonant pumping $(\Omega_1-\omega_{1s})/\Gamma=1.0$. Based on these theoretical results, we will discuss the physical origins of these hierarchical structures and the observed four-wave mixing spectra of GaAs quantum wells in Sec. IV.

III. DIFFERENTIAL TRANSMISSION SPECTRUM

Differential transmission is measured as the transmission change of the probe field $\mathbf{E}_{\text{probe}}(\Omega_2,\mathbf{k}_2)$

$=2\mathbf{E}_2\cos(\Omega_2 t-\mathbf{k}_2\cdot\mathbf{r})$ due to the presence of pump field $\mathbf{E}_{\text{pump}}(\Omega_1,\mathbf{k}_1)=2\mathbf{E}_1\cos(\Omega_1 t-\mathbf{k}_1\cdot\mathbf{r})$ as shown in Fig. 5.

This is described by the third-order optical polarization $P^{(3)}(\Omega_2,\mathbf{k}_2)$:

$$P^{(3)}(\Omega_2,\mathbf{k}_2)=\chi^{(3)}(\Omega_2;\Omega_1,-\Omega_1,\Omega_2)\times\mathbf{E}(\Omega_1)\mathbf{E}(-\Omega_1)\mathbf{E}(\Omega_2)\ , \tag{3.1}$$

where

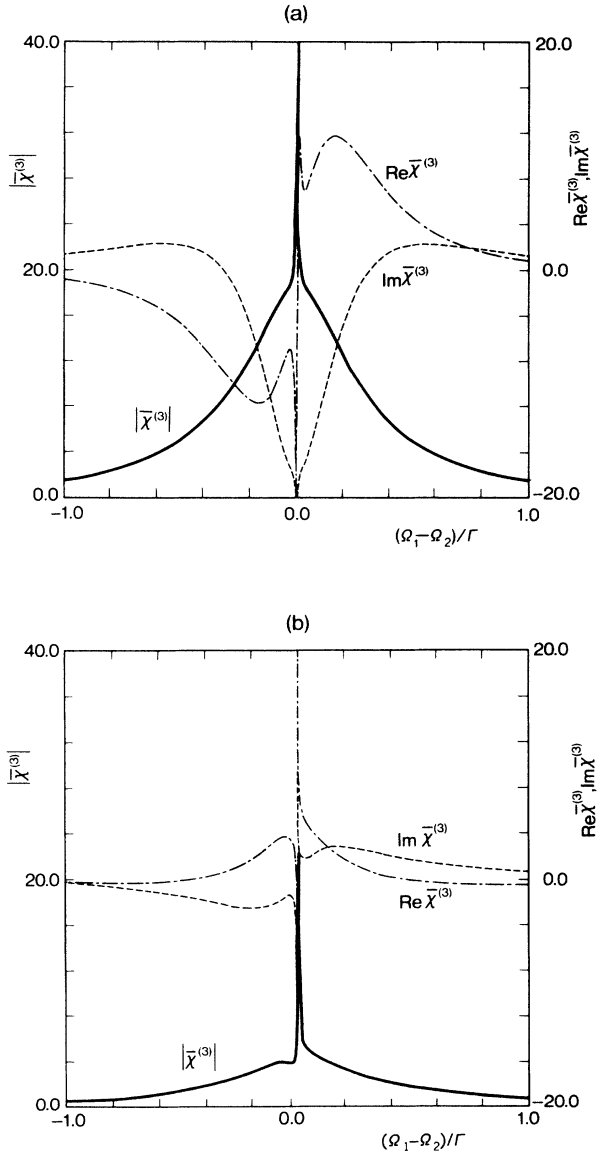

FIG. 4. Four-wave mixing spectra $|\bar{\chi}^{(3)}|\equiv\chi^{(3)}(2\Omega_1-\Omega_2;\Omega_1,-\Omega_2,\Omega_1)|/[|P_{1s}|^4/(\hbar\Gamma)^3]$ are shown by solid lines as a function of detuning $(\Omega_1-\Omega_2)/\Gamma$. Parameters are $\Gamma_{T\to g}/\Gamma=0.001$, $\Gamma_{n\to T}/\Gamma=0.01$, $\gamma/\Gamma=0.1$, and (a) $(\Omega_1-\omega_{1s})/\Gamma=0$ and (b) $(\Omega_1-\omega_{1s})/\Gamma=1.0$. Real and imaginary parts of the normalized third-order optical susceptibility are presented by the dashed-dotted and dotted lines, respectively.

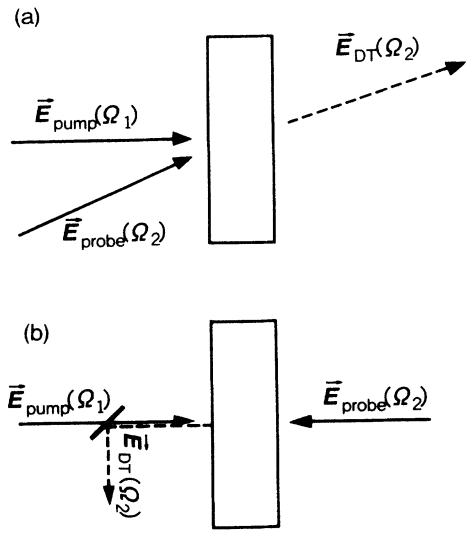

FIG. 5. Schematic of measurement of differential transmission by (a) conventional method and (b) that used by Steel *et al.* (Ref. 11).

$$\mathbf{E}(\pm\Omega_i)=\mathbf{E}_i\exp[\pm i(\Omega_i t-\mathbf{k}_i\cdot\mathbf{r})]\quad(i=1\text{ and }2)\ .$$

In this section, we derive the expression $P^{(3)}(\Omega_2,\mathbf{k}_2)$ by the third-order perturbation in electron-radiation interaction H'. We use the same dipolar approximation for H' as in Sec. II. This differential transmission spectrum is also evaluated under nearly resonant pumping of the lowest-energy exciton, which relaxes possibly into a lower bound state. We use the same five-level model for the electronic system as shown in Fig. 2. The density matrix $\rho(t)$ of the electronic system also obeys the same equations as Eq. (2.1). We present in Fig. 6 the progression of density matrices in each step of the perturbation to third order in H' under the rotating-wave approximation.

(1) In first order in H', we need consider in the present problem the following three components of the density matrices:

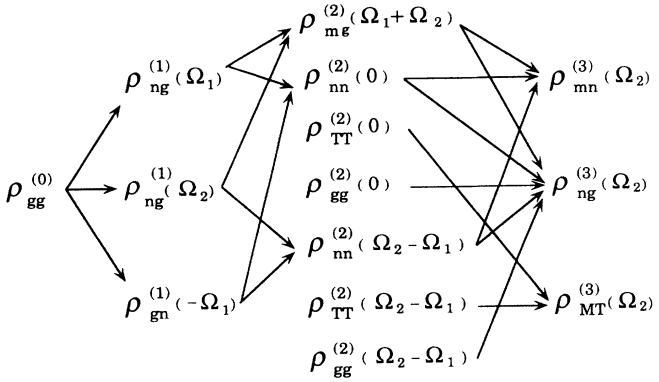

FIG. 6. The development of the density matrix of electronic system due to its perturbation of the external fields with angular frequencies Ω_1 and Ω_2 for differential transmission measurement.

$$\rho_{ng}^{(1)}(\Omega_1)=\frac{H'_{ng}(\Omega_1)\rho_g^{(0)}}{\hbar(\Omega_1-\omega_{ng}+i\Gamma_{ng})} , \tag{3.2}$$

$$\rho_{gn}^{(1)}(-\Omega_1)=\frac{\rho_g^{(0)}H'_{gn}(-\Omega_1)}{\hbar(\Omega_1-\omega_{ng}-i\Gamma_{ng})} , \tag{3.3}$$

$$\rho_{ng}^{(1)}(\Omega_2)=\frac{H'_{ng}(\Omega_2)\rho_g^{(0)}}{\hbar(\Omega_2-\omega_{ng}+i\Gamma_{ng})} . \tag{3.4}$$

(2) The second-order stationary solution of Eq. (2.1) consists of one off-diagonal component $\rho_{mg}^{(2)}(\Omega_1+\Omega_2)$ and six diagonal ones. For example, $\rho_{mg}^{(2)}(\Omega_1+\Omega_2)$ and $\rho_{nn}^{(2)}(\Omega_2-\Omega_1)$ are obtained from Eq. (2.1) as follows:

$$\hbar(\Omega_1+\Omega_2-\omega_{mg}+i\Gamma_{mg})\rho_{mg}^{(2)}(\Omega_1+\Omega_2) =H'_{mn}(\Omega_2)\rho'_{ng}(\Omega_1)+H'_{mn}(\Omega_1)\rho'_{ng}(\Omega_2) , \tag{3.5}$$

$$\hbar(\Omega_2-\Omega_1+i\Gamma_n)\rho_{nn}^{(2)}(\Omega_2-\Omega_1) =H'_{ng}(\Omega_2)\rho_{gn}^{(1)}-(-\Omega_1)\rho_{ng}^{(1)}(\Omega_2)H'_{gn}(-\Omega_1) . \tag{3.6}$$

These density matrices are expressed in the following form:

$$\rho_{mg}^{(2)}(\Omega_1+\Omega_2)=\frac{H'_{mn}(\Omega_2)H'_{ng}(\Omega_1)\rho_{gg}^{(0)}}{\hbar^2(\Omega_1+\Omega_2-\omega_{mg}+i\Gamma_{mg})(\Omega_1-\omega_{mg}+i\Gamma_{ng})}+\frac{H'_{mn}(\Omega_1)H'_{ng}(\Omega_2)\rho_{gg}^{(0)}}{\hbar^2(\Omega_1+\Omega_2-\omega_{mg}+i\Gamma_{mg})(\Omega_2-\omega_{mg}+i\Gamma_{ng})} , \tag{3.7}$$

$$\rho_{nn}^{(2)}(\Omega_2-\Omega_1)=\frac{2\Gamma_{ng}-i(\Omega_2-\Omega_1)}{\Gamma_n-i(\Omega_2-\Omega_1)}\frac{H'_{ng}(\Omega_2)\rho_{gg}^{(0)}H'_{gn}(-\Omega_1)}{\hbar^2(\Omega_2-\omega_{ng}+i\Gamma_{ng})(\Omega_1-\omega_{ng}-i\Gamma_{ng})} . \tag{3.8}$$

The second-order population at the trapped state $|T\rangle$ is obtained from an equation similar to Eq. (2.8):

$$\rho_{TT}^{(2)}(\Omega_2-\Omega_1)=\frac{\Gamma_{n\to T}}{\Gamma_{T\to g}-i(\Omega_2-\Omega_1)}\rho_{nn}^{(2)}(\Omega_2-\Omega_1) . \tag{3.9}$$

The conservation of the population is guaranteed by the following relation which is also obtained from Eq. (2.1):

$$\rho_{gg}^{(2)}(\Omega_2-\Omega_1)=-\rho_{nn}^{(2)}(\Omega_2-\Omega_1)-\rho_{TT}^{(2)}(\Omega_2-\Omega_1) . \tag{3.10}$$

Three other components are given by replacing Ω_2 by Ω_1 in Eqs. (3.8)–(3.10), as follows:

$$\rho_{nn}^{(2)}(0)=\frac{2\Gamma_{ng}}{\Gamma_n}\frac{H'_{ng}(\Omega_1)\rho_{gg}^{(0)}H'_{gn}(-\Omega_1)}{\hbar^2(\Omega_1-\omega_{ng}+i\Gamma_{ng})(\Omega_1-\omega_{ng}-i\Gamma_{ng})} , \tag{3.11}$$

$$\rho_{TT}^{(2)}(\Omega_2-\Omega_1)=\frac{\Gamma_{n\to T}}{\Gamma_{T\to g}}\rho_{nn}^{(2)}(0) , \tag{3.12}$$

$$\rho_{gg}^{(2)}(0)=-\rho_{nn}^{(2)}(0)-\rho_{TT}^{(2)}(0) . \tag{3.13}$$

(3) To third order in H', three off-diagonal components $\rho_{ng}^{(3)}(\Omega_2)$, $\rho_{mn}^{(3)}(\Omega_2)$, and $\rho_{MT}^{(3)}(\Omega_2)$ are obtained by solving the following equations for the density matrices:

$$\hbar(\Omega_2-\omega_{ng}+i\Gamma_{ng})\rho_{ng}^{(3)}(\Omega_2)=H'_{nm}(-\Omega_1)\rho_{mg}^{(2)}(\Omega_1+\Omega_2)+H'_{ng}(\Omega_2)\rho_{gg}^{(2)}(0) +H'_{ng}(\Omega_1)\rho_{gg}^{(2)}(\Omega_2-\Omega_1)-\rho_{nn}^{(2)}(0)H'_{ng}(\Omega_2)-\rho_{nn}^{(2)}(\Omega_2-\Omega_1)H'_{ng}(\Omega_1) , \tag{3.14}$$

$$\hbar(\Omega_2-\omega_{mn}+i\Gamma_{mn})\rho_{mn}^{(3)}(\Omega_2)=H'_{mn}(\Omega_2)\rho_{nm}^{(2)}(0)+H'_{mn}(\Omega_1)\rho_{nn}^{(2)}(\Omega_2-\Omega_1)-\rho_{mg}^{(2)}(\Omega_1+\Omega_2)H'_{gn}(-\Omega_1) , \tag{3.15}$$

$$\hbar(\Omega_2-\omega_{MT}+i\Gamma_{MT})\rho_{MT}^{(3)}(\Omega_2)=H'_{MT}(\Omega_2)\rho_{TT}^{(2)}(0)+H'_{MT}(\Omega_1)\rho_{TT}^{(2)}(\Omega_2-\Omega_1) . \tag{3.16}$$

When we are interested only in the nearly resonant pumping of the lowest-energy exciton with the largest oscillator strength, we may choose single- and two-exciton states, respectively, for one- and two-excitation states $|n\rangle$ and $|m\rangle$. Here we must distinguish between two cases of two-exciton state $|m\rangle$: (1) two excitons with the same spin structure are excited and (2) those with different spin structure for which the bound state of the EM is formed. As mentioned already in Sec. II, the second contribution is negligible for the following two cases: (a) the coherent length of the exciton is much larger than the average separation a_m of two excitons in the EM, e.g., for excitons in pure GaAs quantum wells at low temperature,[25–27] and (b) the molecular binding energy $\hbar\omega_m^b$ is much larger than the excitonic homogeneous broadening $\hbar\Gamma$ and the 1s exciton is nearly resonantly pumped, e.g., for excitons in bulk CuCl crystal[28] and CuCl microcrystallites.[29] Furthermore the contribution of the trapped state to the absorption saturation and differential transmission spectra is dominant over the intrinsic contribution near the degenerate case $\Omega_2=\Omega_1$. We are interested here in the singular behavior of the differential transmission spec-

trum around this frequency region. Therefore, we confine ourselves to the case in which two excitons in the $|m\rangle$ state have the same spin structure in the bulk crystal or quantum-well system, so that the repulsive interaction $\hbar\omega_{\rm int}$ between two excitons is negligible in comparison to $\hbar\Gamma$. As a result, we can choose the eigenenergies, the transition dipole moments, and the relaxation constants as follows:

$$\omega_{ng}=\omega_{1s},\quad \omega_{mg}=2\omega_{1s},\quad \omega_{mn}=\omega_{1s}\ ,$$
$$P_{ng}=P_{1s},\quad P_{mn}=\sqrt{2}P_{1s}\ ,$$

and

$$\Gamma_n=2\gamma,\quad \Gamma_{ng}=\Gamma,\quad \Gamma_{mg}=2\Gamma,\quad \Gamma_{mn}=\Gamma+2\gamma\ . \tag{3.17}$$

Then we can represent the differential transmission spectrum in lowest order both in the pump and probe fields in terms of $-\mathrm{Im}\langle P^{(3)}(\Omega_2)\rangle$. Here

$$\begin{aligned}
\langle P^{(3)}(\Omega_2)\rangle &= \mathrm{Tr}\langle P\rho^{(3)}(\Omega_2)\rangle \\
&= P_{gn}\rho^{(3)}_{ng}(\Omega_2)+P_{nm}\rho^{(3)}_{mn}(\Omega_2)+\sum_M P_{TM}\rho^{(3)}_{MT}(\Omega_2) \\
&= \frac{P_{gn}H'_{nm}(-\Omega_1)H'_{mn}(\Omega_2)H'_{ng}(\Omega_1)\rho^{(0)}_{gg}}{\hbar^3(\Omega_2-\omega_{ng}+i\Gamma_{ng})(\Omega_1+\Omega_2-\omega_{mg}+i\Gamma_{mg})(\Omega_1-\omega_{ng}+i\Gamma_{ng})} \\
&\quad+\frac{P_{gn}H'_{nm}(-\Omega_1)H'_{mn}(\Omega_1)H'_{ng}(\Omega_2)\rho^{(0)}_{gg}}{\hbar^3(\Omega_2-\omega_{ng}+i\Gamma_{ng})^2(\Omega_1+\Omega_2-\omega_{mg}+i\Gamma_{mg})} \\
&\quad-\frac{4\Gamma_{ng}P_{gn}H'_{ng}(\Omega_1)\rho^{(0)}_{gg}H'_{gn}(-\Omega_1)H'_{ng}(\Omega_2)}{\hbar^3\Gamma_n(\Omega_2-\omega_{ng}+i\Gamma_{ng})[(\Omega_1-\omega_{ng})^2+\Gamma^2_{ng}]} \\
&\quad-\frac{2[2\Gamma_{ng}-i(\Omega_2-\Omega_1)]P_{gn}H'_{ng}(\Omega_2)\rho^{(0)}_{gg}H'_{gn}(-\Omega_1)H'_{ng}(\Omega_1)}{\hbar^3[\Gamma_n-i(\Omega_2-\Omega_1)](\Omega_2-\omega_{ng}+i\Gamma_{ng})^2(\Omega_1-\omega_{ng}-i\Gamma_{ng})} \\
&\quad+\frac{2\Gamma_{ng}P_{nm}H'_{mn}(\Omega_2)H'_{ng}(\Omega_1)\rho^{(0)}_{gg}H'_{gn}(-\Omega_1)}{\hbar^3\Gamma_n(\Omega_2-\omega_{mn}+i\Gamma_{mn})[(\Omega_1-\omega_{ng})^2+\Gamma^2_{ng}]} \\
&\quad+\frac{[2\Gamma_{ng}-i(\Omega_2-\Omega_1)]P_{nm}H'_{mn}(\Omega_1)H'_{ng}(\Omega_2)\rho^{(0)}_{gg}H'_{gn}(-\Omega_1)}{\hbar^3[\Gamma_n-i(\Omega_2-\Omega_1)](\Omega_2-\omega_{mn}+i\Gamma_{mn})(\Omega_2-\omega_{ng}+i\Gamma_{ng})(\Omega_1-\omega_{ng}-i\Gamma_{ng})} \\
&\quad-\frac{P_{nm}H'_{mn}(\Omega_2)H'_{ng}(\Omega_1)\rho^{(0)}_{gg}H'_{gn}(-\Omega_1)}{\hbar^3(\Omega_2-\omega_{mn}+i\Gamma_{mn})(\Omega_1+\Omega_2-\omega_{mg}+i\Gamma_{mg})(\Omega_1-\omega_{ng}+i\Gamma_{ng})} \\
&\quad-\frac{P_{nm}H'_{mn}(\Omega_1)H'_{ng}(\Omega_2)\rho^{(0)}_{gg}H'_{gn}(-\Omega_1)}{\hbar^3(\Omega_2-\omega_{mn}+i\Gamma_{mn})(\Omega_1+\Omega_2-\omega_{mg}+i\Gamma_{mg})(\Omega_2-\omega_{ng}+i\Gamma_{ng})} \\
&\quad+\frac{2\Gamma_{n\to T}\Gamma_{ng}H'_{ng}(\Omega_1)\rho^{(0)}_{gg}H'_{gn}(-\Omega_1)}{\hbar^3\Gamma_{T\to g}\Gamma_n[(\Omega_1-\omega_{ng})^2+\Gamma^2_{ng}]}\left[\sum_M\frac{P_{TM}H'_{MT}(\Omega_2)}{\Omega_2-\omega_{MT}+i\Gamma_{MT}}-\frac{P_{gn}H'_{ng}(\Omega_2)}{\Omega_2-\omega_{ng}+i\Gamma_{ng}}\right] \\
&\quad+\frac{\Gamma_{n\to T}[2\Gamma_{ng}-i(\Omega_2-\Omega_1)]H'_{ng}(\Omega_2)\rho^{(0)}_{gg}H'_{gn}(-\Omega_1)}{\hbar^3[\Gamma_{T\to g}-i(\Omega_2-\Omega_1)][\Gamma_n-i(\Omega_2-\Omega_1)]}\left[\sum_M\frac{P_{TM}H'_{MT}(\Omega_1)}{\Omega_2-\omega_{MT}+i\Gamma_{MT}}-\frac{P_{gn}H'_{ng}(\Omega_1)}{\Omega_2-\omega_{ng}+i\Gamma_{ng}}\right]\ .
\end{aligned} \tag{3.18}$$

This is rewritten in the nondimensional form by scaling all frequencies and relaxation constants to Γ:

$$(\Omega_2-\Omega_1)/\Gamma\equiv x,\quad (\Omega_1-\omega_{1s})/\Gamma\equiv y,\quad \gamma/\Gamma\equiv\gamma,\quad \Gamma_{n\to T}/\Gamma\equiv\gamma_{n\to T},\quad \Gamma_{T\to g}/\Gamma\equiv\gamma_{T\to g},$$
$$\Gamma_{MT}/\Gamma\equiv\gamma_{MT},\quad -\sum_M\left[\frac{P_{MT}}{P_{1s}}\right]^2\frac{1}{(\Omega_2-\omega_{MT})/\Gamma+i\gamma_{MT}}\equiv -A+iB\ , \tag{3.19}$$

$$\langle P^{(3)}(x)\rangle/\{|P_{1s}|^4E(\Omega_2)|E(\Omega_1)|^2/(\hbar\Gamma)^3\}=-\frac{1}{(x+y+i)(x+2y+2i)}\left[\frac{1}{y+i}+\frac{1}{x+i}\right]$$
$$+\frac{2}{\gamma(y^2+1)(x+y+i)}+\frac{2(2-ix)}{(2\gamma-ix)(x+y+i)^2(y-i)}$$
$$-\frac{1}{\gamma(y^2+1)[x+y+i(1+2\gamma)]}$$
$$-\frac{2-ix}{(2\gamma-ix)[x+y+i(1+2\gamma)](x+y+i)(y-i)}$$
$$+\frac{1}{[x+y+i(1+2\gamma)](x+2y+2i)}\left[\frac{1}{y+i}+\frac{1}{x+y+i}\right]$$
$$+\frac{\gamma_{n\to T}}{\gamma\gamma_{T\to g}(y^2+1)}\left[-A+iB+\frac{1}{x+y+i}\right]$$
$$+\frac{\gamma_{n\to T}(2-ix)}{(2\gamma-ix)(\gamma_{T\to g}-ix)(x+y+i)(y-i)}\left[-A+iB+\frac{1}{x+y+i}\right]. \tag{3.20}$$

The last term of Eqs. (3.18) and (3.20) describes the main effect of the bound state on the differential transmission spectrum. This has two factors $[\Gamma_{T\to g}-i(\Omega_2-\Omega_1)]$ and $[\Gamma_n-i(\Omega_2-\Omega_1)]$ in the denominator. The linear polarizability $-A+iB$ of the trapped state is given by Eq. (3.19). The decay rates $\Gamma_{T\to g}$ and Γ_n are, respectively, the smallest around the second smallest constants so that $-\mathrm{Im}\langle P^{(3)}(\Omega_2)\rangle$ has the very large spike or dip as a function of $\Omega_2-\Omega_1$ and $\Omega_2-\Omega_1=0$, depending upon the sign of $B-1/[(x+y)^2+1]$. The higher excited states $|M\rangle$ constitute the continuum so that the summation over M reduces A and B to be a constant almost independent of Ω_2 around $\Omega_2=\omega_{1s}$. We calculate the differential transmission spectrum $-\mathrm{Im}\langle P^{(3)}(\Omega_2)\rangle$ by choosing $A=0$ and $B=0.25$ and $y\equiv(\Omega_1-\omega_{1s})/\Gamma=-2.0$, 0.0, and 2.0, as shown in Fig. 7.

As Fig. 7(b) shows, $-\mathrm{Im}\langle P^{(3)}(\Omega_2)\rangle$ has a positive peak around $x=(\Omega_2-\Omega_1)/\Gamma=0$ with the width $2\gamma/\Gamma$ when $y=(\Omega_1-\omega_{1s})/\Gamma=0$. This positive peak $-\mathrm{Im}\langle P^{(3)}(\Omega_2)\rangle>0$ means the absorption saturation. This is due to the fact that the absorption saturation of the exciton $-1/[(x+y)^2+1]$ overcomes the induced absorption B of the trapped state in the brackets in the last two terms of Eq. (3.20). On the other hand, it changes into the dip with some asymmetry with both sides, when $y=(\Omega_1-\omega_{1s})/\Gamma=\pm2$, corresponding to $B-1/[(x+y)^2+1]>0$ around $x=0$. The sharp dip has the spectrum with $2\gamma_{T\to g}/\Gamma$ and means that the induced absorption due to the trapped state is overwhelming. This kind of spectrum change has been observed on the exciton in PbI_2 crystal with different assignments.[30] This will be discussed in Sec. IV.

IV. DISCUSSIONS

The third-order optical nonlinearity causes a great variety of phenomena. In this paper, we have discussed several effects of the excitonic trapped state on the third-order nonlinear optical responses. First, we discussed in Sec. II the nearly degenerate four-wave mixing under nearly resonant pumping of the exciton with two beams, and the generation of the phase-conjugated wave with three beams. The signal for both of these phenomena is

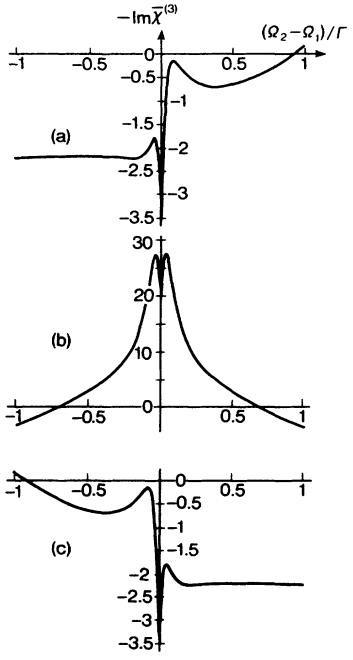

FIG. 7. Differential transmission spectrum $-\mathrm{Im}\bar{\chi}^{(3)}\equiv-\mathrm{Im}\langle P^{(3)}(\Omega_2)\rangle/\{|P_{1s}|^4E(\Omega_2)|E(\Omega_1)|^2/(\hbar\Gamma)^3\}$ under nearly resonant pumping of the 1s exciton: $(\Omega_1-\omega_{1s})/\Gamma=-2.0$ (a), 0.0 (b), and 2.0 (c). Chosen relaxation constants and linear polarizability $-A+iB$ of the trapped state are $\gamma/\Gamma=0.1$, $\Gamma_{n\to T}/\Gamma=0.05$, $\Gamma_{T\to g}/\Gamma=0.02$, and $-A+iB=0.25i$.

proportional to the square of the absolute value of the third-order optical susceptibilities $\chi^{(3)}(2\Omega_1-\Omega_2;\Omega_1,-\Omega_2,\Omega_1)$. Although both real and imaginary parts of $\chi^{(3)}$are accompanied by complicated structures as Figs. 4(a) and 4(b) show, the spectrum of the absolute value of $\chi^{(3)}$ is rather simple but has a hierarchical structure due to the presence of the excitonic trapped state. Usually the trapped state has the longest decay time $\tau_{T\to g}=(\Gamma_{T\to g})^{-1}$ so that the sharpest peak of $|\chi^{(3)}|$ appears at $\Omega_1-\Omega_2=0$. The exciton has the second longest decay time $\tau_n=(\Gamma_n)^{-1}$. As Figs. 4(a) and 4(b) as well as Eq. (2.33) and (2.34) show, the spectrum of $|\chi^{(3)}|$ has also the Lorentzian shape with width Γ_n around $\Omega_1-\Omega_2=0$. The relaxation constant Γ_{ng} of the excitonic polarization is the largest. As a result, the signal of the four-wave mixing as well as the generation of the phase-conjugated wave, which is described by the square of $|\chi^{(3)}|$, has broad enhancement around $\Omega_1\approx\omega_{ng}$ as well as $\Omega_2\approx\omega_{ng}$ as Eqs. (2.33) and (2.34) show.

On the other hand, the differential transmission spectrum is described by the imaginary part of $\chi^{(3)}(\Omega_2;\Omega_1,-\Omega_1,\Omega_2)$. Depending upon the pump frequency Ω_1 relative to ω_{ng}, i.e., the magnitude of the absorption coefficient of Ω_2 from the trapped state into the higher excited state relative to that from the ground state to the excited one $|n\rangle$, the differential transmission spectrum changes from the induced absorption to the absorption saturation, i.e., from the dip to the spike, as Figs. 7 show. The polarization rotation spectrum under the pump-probe method is not represented by the absolute value of $\chi^{(3)}$ but by the real and imaginary parts of $\chi^{(3)}$ in a complicated way. Therefore, we can expect the dip and spike structures around $\Omega_1=\Omega_2$ depending upon the pump frequency Ω_1 relative to ω_{ng} in the polarization rotation spectrum of the linearly polarized probe light under pumping by the circularly polarized pump beam.

Remillard and his co-workers measured cw frequency-domain four-wave mixing mainly due to the $n=1$ heavy-hole exciton in GaAs multiple quantum wells, and observed that the excitation relaxation consist of both fast and slow components.[24] This was made possible by the high-resolution spectroscopy measurements of frequency-domain four-wave mixing as a function of detuning $\Omega_1-\Omega_2$. They observed three resonances with linewidths of 3 GHz, 10 MHz, and 30 kHz, which correspond to the lifetimes 100 psec, 30 nsec, and 10 μsec, respectively. We may tentatively assign those hierarchical structures in terms of the present model as follows. The sharpest spike with the linewidth 30 kHz corresponds to the spike in Fig. 4, the linewidth of which is determined by $\Gamma_{T\to g}$. This looks reasonable as the lifetime of the trapped state is considered to be on the order of microseconds. The second sharpest structure, with linewidth 10 MHz, also with the center at $\Omega_1-\Omega_2=0$ comes from the excitonic lifetime $(\Gamma_n)^{-1}$, on the order of nanoseconds. The widest structure, with width 3 GHz, is not clearly assigned but the present model suggests this broad band to come from the dephasing Γ_{ng} of the excitonic polarization.

The differential transmission spectrum was observed[30] for the exciton in PbI_2 crystal to change around $\Omega_1=\Omega_2$ from the dispersive type under off-resonant pumping of the exciton $|\Omega_1-\omega_{1s}|>\Gamma$ on both the sides into the negative induced absorption line with symmetric shape at the resonant pumping $|\Omega_1-\omega_{1s}|=0$. These had been analyzed[30] by the conventional $\chi^{(3)}$ expression for the intrinsic system. We consider, however, the ability to properly understand these features only by taking into account the effects of the trapped state as shown in Fig. 7. The effects of the trapped state on the differential transmission spectrum are represented mainly by the last two terms of Eq. (3.18). The contribution of the last term, in particular, is extremely enhanced when the detuning $|\Omega_1-\Omega_2|$ of two beams is reduced to less than the exciton spectrum width Γ. This is because the decay rate $\Gamma_{T\to g}$ of the trapped state into the ground state is the smallest and the decay rate Γ_n of the exciton is the second smallest among the inverse of the characteristic time constants, so that the population $\rho_{TT}(\Omega_2-\Omega_1)$ of the trapped state increases under $|\Omega_2-\Omega_1|<\Gamma_{T\to g}$, and $|\Omega_2-\Omega_1|<\Gamma_n$ as Eq. (3.18) show.

The sign of the transmission spectrum around $(\Omega_2-\Omega_1)/\Gamma=0$ depends on the relative magnitude of the excitonic absorption to the induced absorption from the trapped state to the higher excited state. Therefore, we expect the absorption saturation, i.e., the negative induced absorption due to the $1s$ exciton with the symmetric broadening as shown in Fig. 7(b) at the resonant pumping $|\Omega_1-\omega_{1s}|=0$. This changes into induced absorption for off-resonant pumping of the exciton $|\Omega_1-\omega_{1s}|/\Gamma=2$ because the induced absorption from the trapped state T to the higher excited state M is almost independent of Ω_2 around $\Omega_2\sim\Omega_1\sim\omega_{1s}$ as the M states are continuously distributed but the excitonic absorption is reduced to $\frac{1}{5}$ of the peak value at the off-resonant pumping, as Figs. 7(a) and 7(c) show. Here the differential transmission spectrum becomes negative around $|\Omega_2-\Omega_1|/\Gamma=0$. This means that the induced absorption overcomes under the off-resonant pumping $|\Omega_1-\omega_{1s}|/\Gamma=2$. The differential transmission spectrum around the origin of $(\Omega_2-\Omega_1)$ consists of two structures. The first one is the sharp induced absorption line with the smallest spectrum width $\Gamma_{T\to g}$. The second is a combined structure of the dispersive type and the absorption saturation both with the spectrum width Γ_n as Figs. 7(a) and 7(c) show. Note that the left- and right-hand structures are exchanged with respect to the origin $(\Omega_2-\Omega_1)/\Gamma=0$ for the pumping $(\Omega_1-\omega_{1s}=2\Gamma)$ above the exciton ω_{1s} [Fig. 4(a)] and $(\Omega_1-\omega_{1s}=-2\Gamma)$ below one [Fig. 4(c)]. The relative depth of the sharp dip depends on the ratio of $\Gamma_{n\to T}$ to Γ_n. The trapping rate $\Gamma_{n\to T}$ is determined by the concentration of the impurities and the cross section of trapping the exciton at the impurity.

Finally, we list the problems remaining unsolved in the present paper. First, we discussed the stationary responses of the third-order nonlinear optical phenomena in this paper. When we, however, use the short laser pulses, as short as picosecond or femtosecond magnitude, we need to solve the equations of motion for the density

matrix as a function of time. The signal intensity as well as the spectrum of four-wave mixing and differential transmission depend sensitively on the relative time at which the pump and probe beams are applied. This is a future problem. Second, we do not yet know the microscopic structure of the trapped state, e.g., in the semiconductor microcrystallite of CuCl and $CdS_{1-x}Se_x$ embedded in insulators or glasses. We believe that the donors or acceptors, or the isoelectric traps, will play the roles of the trapped states of the exciton in bulk crystals, e.g., in PbI_2 and CuCl crystal. The surface fluctuations of the GaAs quantum-well system also may represent the trapping center of excitons. While we are calculating microscopically the surface-trapped states in the semiconductor microscrystallites, the origin of the trapped state may be partially solved experimentally by observing the present four-wave mixing spectrum or the differential transmission spectrum while controlling the concentration of impurities.

ACKNOWLEDGMENTS

The author is grateful to D. G. Steel, M. Gonokami, T. Taniguchi, and J. Haus for fruitful discussions. This work was financially supported by a Grant-in-Aid from the Ministry of Education, Science, and Culture of Japan. This is also part of the cooperative research between Japan and the U.S.A. supported by Japan Promotion of Sciences and NEDO's International Joint Research Program on "Ultrafast Nonlinear Optical Response of Semiconductor Quantum Structures and its Application to Ultrafast Optical Information Processing."

[1]Y. R. Shen, *The Principles of Nonlinear Optics* (Wiley, New York, 1984), Chap. 14.

[2]E. Hanamura, Phys. Rev. B **37**, 1273 (1988).

[3]Y. Masumoto, M. Yamazaki, and H. Sugawara, Appl. Phys. Lett. **53**, 1527 (1988).

[4]A. Nakamura, in *Proceedings of 5th Toyota Conference on Nonlinear Optical Materials,* edited by S. Miyata (Elsevier, Oxford, 1991); A. Nakamura, T. Tokizaki, and T. Kataoka (unpublished).

[5]T. Saiki, K. Takeuchi, M. Kuwata-Gonokami, T. Mitsuyu, and K. Ohkawa, Appl. Phys. Lett. **60**, 192 (1992).

[6]M. A. Lampert, Phys. Rev. Lett. **1**, 450 (1958).

[7]For example, see references in H. Kukimoto, S. Shionoya, S. Toyotomi, and K. Morigaki, J. Phys. Soc. Jpn. **28**, 110 (1970).

[8]T. Arai, H. Fujumura, I. Umezu, T. Ogawa, and A. Fujii, Jpn. J. Appl. Phys. **28**, 484 (1989).

[9]T. Itoh (unpublished).

[10]M. Tomita and M. Matsuoka, J. Opt. Soc. Am. B **7**, 1198 (1990).

[11]D. G. Steel, P. K. Bhattacharya, J. T. Remillard, Hailin Wang, M. D. Webb, J. Pamulapatti, and J. Oh (unpublished).

[12]D. H. Auston *et al.*, Appl. Opt. **26**, 211 (1987).

[13]See, e.g., Y. R. Shen, *The Principles of Nonlinear Optics* (Ref. 1), Chap. 2.

[14]E. Hanamura, Phys. Rev. B **38**, 1228 (1988).

[15]T. Itoh, F. Jin, Y. Iwabuchi, and T. Ikehara, in *Nonlinear Optics of Organics and Semiconductors,* edited by T. Kobayashi, Springer Proceedings in Physics Vol. 36 (Springer-Verlag, Berlin, 1989), p. 76.

[16]T. Takagawara, Phys. Rev. B **39**, 10 206 (1989).

[17]Y. Z. Hu, M. Lindberg, and S. W. Koch, Phys. Rev. B **42**, 1713 (1990); see also Y. Z. Hu, S. W. Koch, M. Lindberg, N. Peyghambarian, R. Pollock, and F. F. Abraham, Phys. Rev. Lett. **64**, 1805 (1990).

[18]E. Hanamura, Proc. SPIE **1268**, 96 (1990).

[19]E. Hanamura, M. Gonokami, and H. Ezaki, Solid State Commun. **73**, 551 (1990).

[20]E. Hanamura, in *Proceedings of International Conference on Noncrystalline Solids,* edited by L. D. Pye (Taylor & Francis, London, 1991); in *Proceedings of 5th Toyota Conference on Nonlinear Optical Materials* (Ref. 4).

[21]E. Hanamura, Solid State Commun. **12**, 951 (1973).

[22]E. I. Rashba, in *Excitons at High Density,* edited by H. Haken and S. Nikitine, Springer Tracts in Modern Physics Vol. 73 (Springer-Verlag, Berlin, 1975), p. 150.

[23]J. Feldman, G. Peter, E. O. Göbel, P. Dawson, K. Moore, C. Foxen, and R. J. Elliott, Phys. Rev. Lett. **59**, 2337 (1987).

[24]J. T. Remillard, H. Wang, D. G. Steel, J. Oh, J Pamulapati, and P. K. Bhattacharya, Phys. Rev. Lett. **62**, 2861 (1989).

[25]B. F. Feuerbacher, J. Kuhl, and K. Ploog, Phys. Rev. B **43**, 2439 (1991).

[26]R. Raj, I. Abram, and J. A. Levenson, Superlatt. Microstruct. **10**, 437 (1991); Solid State Commun. **81**, 51 (1992).

[27]O. Akimoto and E. Hanamura, J. Phys. Soc. Jpn. **23**, 1537 (1972).

[28]M. Ueta, T. Mita, and T. Itoh, Solid State Commun. **32**, 43 (1979).

[29]T. Wamura, Y. Masumoto, and T. Kawamura, Appl. Phys. Lett. **59**, 1758 (1991).

[30]T. Ishihara and T. Goto, J. Phys. Soc. Jpn. **57**, 2191 (1988).